NASA TECHNICAL NOTE

NASA TN D-2385

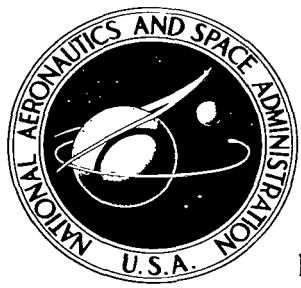

LOAN COPY: RETL
AFWL (WLIL-
KIRTLAND AFB, N

01549 31

TECH LIBRARY KAFB, NM

NASA TN D-2385

COMPARISON OF HEAT-REJECTION AND WEIGHT CHARACTERISTICS OF SEVERAL RADIATOR FIN-TUBE CONFIGURATIONS

by Henry C. Haller

Lewis Research Center
Cleveland, Ohio

NATIONAL AERONAUTICS AND SPACE ADMINISTRATION • WASHINGTON, D. C. • JULY 1964

TECH LIBRARY KAFB, NM
0154931

COMPARISON OF HEAT-REJECTION AND WEIGHT CHARACTERISTICS OF SEVERAL RADIATOR FIN-TUBE CONFIGURATIONS

By Henry C. Haller

Lewis Research Center
Cleveland, Ohio

NATIONAL AERONAUTICS AND SPACE ADMINISTRATION

For sale by the Office of Technical Services, Department of Commerce,
Washington, D.C. 20230 -- Price $1.00

COMPARISON OF HEAT-REJECTION AND WEIGHT CHARACTERISTICS OF SEVERAL RADIATOR FIN-TUBE CONFIGURATIONS

by Henry C. Haller

Lewis Research Center

SUMMARY

An analytical investigation was performed to provide comparisons of heat-rejection and weight capabilities of several radiator fin-tube configurations: a central fin and tube, an open-sandwich fin and tube without a fillet, two open-sandwich configurations with fillets, and a closed-sandwich fin and tube with varying side-wall thickness and vulnerable area criterion. Numerical results were obtained for the thermal characteristics of each configuration for the assumptions of isothermal tubes and constant-thickness fins that act as blackbodies radiating from both sides to a space environment at absolute zero.

A 1-megawatt high-temperature Rankine system was chosen for the weight comparison that used maximum heat rejected per unit weight as the evaluating parameter. Results indicate that a substantial weight saving can be realized with the closed-sandwich fin-tube arrangement if the tube side-wall thickness can be reduced as a result of a possible meteoroid bumper effect of the enclosing fins. The heat loss per unit weight for the other fin-tube configurations investigated was of similar magnitude and less than that of the closed-sandwich configuration. Radiator planform area and fin thickness were also investigated.

INTRODUCTION

The available literature yields a wide variety of investigations concerning the radiative characteristics of fin-and-tube radiators for spacecraft and space powerplant applications. Initial studies considered only heat-rejection and weight characteristics of the fin with no interaction between tube and fin (refs. 1 to 5). Radiators of practical interest, however, consist of fin-tube geometries in which there is substantial radiant interaction between radiator elements. Reference 6 is representative of an analytical treatment of the heat-rejection aspects of a central-fin-and-tube geometry. The central-fin-and-tube radiator is analyzed on the basis of heat rejection per unit weight for typical power and temperature levels in references 7 to 10. Other fin-tube arrangements, such as the open sandwich without a fillet, are analyzed in

reference 10. These results, however, may contain some degree of uncertainty because the angle factors in the radiant interchange analysis were not correctly derived, as pointed out in reference 11.

In practice, other variations of the fin-tube arrangement are possible because of considerations relating to fabrication techniques, structural requirements, and meteoroid protection. Heat transfer in several idealized geometries (square tubes) was analyzed (ref. 12) but the weight of the tube was not included in the analysis or in the ultimate comparison of the results.

The aim of this investigation is to provide basic information on heat transfer and total weight and comparisons for five fin-tube configurations: central fin and tube, open-sandwich fin and tube without a fillet, open-sandwich fin and tube with a fillet, open-sandwich fin and tube with a fillet and reduced tube armor thickness, and closed-sandwich fin and tube. In addition, other aspects of radiator specifications, such as planform area and fin and tube physical dimensions, are investigated.

A fin having a rectangular cross section was chosen for this comparison. In all cases cited, a one-dimensional approach was taken in the development of the fin energy-balance equation with the assumption that the base temperature of the fin was equal to the surface temperature of the tube outer wall. The radiator fin-tube weight analysis and the comparisons were carried out for a 1-megawatt high-temperature Rankine power cycle.

The analysis makes no provisions for vapor and liquid headers or pressure-drop considerations for the fluid-carrying tubes. The resultant programs treat the inside tube diameter, fin root and tube base-surface temperature, heat-rejection rate, material properties, mission parameters, and meteoroid protection criteria as the input variables for each geometric configuration.

SYMBOLS

A surface area, sq ft

A_p radiator planform area, sq ft

A_v vulnerable area, sq ft

a penetration correction factor (eq. (15))

c velocity of sound in material, $\sqrt{E_a g/\rho_a}$, ft/sec

D tube diameter, ft

E_a Young's modulus, lb/sq ft

F angle factor, fraction of energy leaving surface that is incident upon another surface

g	acceleration due to gravity, ft/sec^2
h	base-surface length in closed-sandwich configuration, ft
k	thermal conductivity, $Btu/(hr)(ft)(^oR)$
L	minimum fin half-length, $L^* - R_o$, ft
L^*	one-half the tube center-to-center distance, ft
l	actual fin half-length, ft
N_c	conductance parameter, $\sigma l^2 T_b^3/kt$
$P(0)$	probability of zero punctures (eq. (15))
P_e	powerplant output, Mw
Q	heat flow, Btu/hr
R	tube radius, ft
T	temperature, ^oR
t	half-thickness of fin
$\overline{V}$	average meteoroid velocity, ft/sec
W	weight of fin and tube, lb
X	normalized distance coordinate, x/L or x/l
x	coordinate measuring distance along fin, ft
Y	normalized distance coordinate, y/l
y	coordinate measuring distance along fin, ft
Z	radiator tube length, ft
α,β	constants in penetration formula (eq. (15))
δ	tube wall thickness, ft
η	thermal efficiency
η_c	cycle efficiency
η^*	thermal effectiveness
θ	normalized temperature distribution, T/T_b

ρ	density, lb/cu ft (unless otherwise specified)
σ	Stefan-Boltzmann constant, 0.173×10^{-8} Btu/(hr)(sq ft)($^{\circ}R^4$)
τ	mission exposure time, days
φ^*,φ^{**}	angles in fig. 22

Subscripts:

a	armor
b	base surface
c	liner
cond	conduction
f	fin
i	inside
max	maximum
n	net
o	outside
p	particle
R	overall
rad	radiation
s	side wall
1	base surface 1
2	base surface 2

HEAT-TRANSFER ANALYSIS AND RESULTS

General Considerations

The analysis considers the thermal characteristics of the central-fin, open-sandwich, and closed-sandwich configurations shown in figure 1. Each tube is composed of a thin inner liner of thickness δ_c surrounded by meteoroid armor of thickness δ_a, and the tubes are connected by a fin surface. The closed-sandwich configuration of figure 1(e) is assigned various values of side-wall thickness to allow for a reduction in armor thickness that might be possible as a result of the bumper action of the fin. The fin thickness for

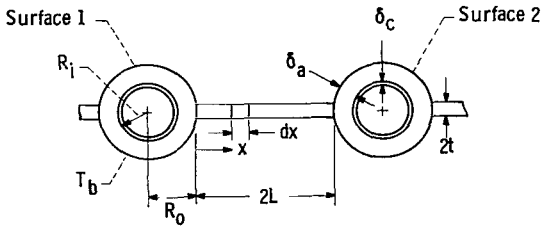

(a) Central fin and tube; $l = L$.

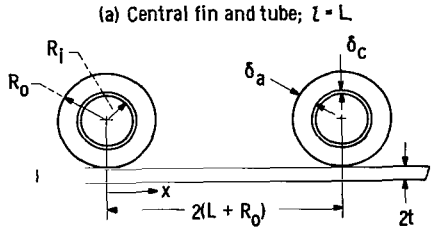

(b) Open-sandwich fin and tube without fillet; $l = L + R_o$.

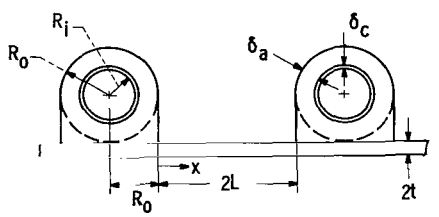

(c) Open-sandwich fin and tube with fillet, type A; $l = L$.

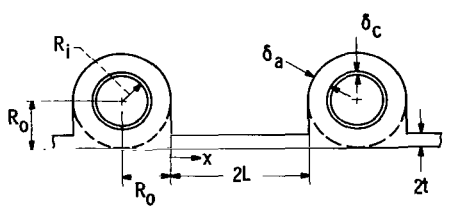

(d) Open-sandwich fin and tube with fillet, type B; $l = L$.

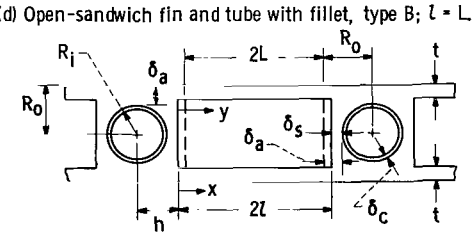

(e) Closed-sandwich fin and tube with variable side wall; $l = L + \delta_a(1 - \delta_s/\delta_a)$.

Figure 1. - Radiator fin-tube configurations studied.

this configuration is one-half of the fin thickness of the other configurations. (Principal symbols and dimensions are shown in fig. 1.)

The governing differential equations that yield the fin temperature profiles and their solutions are given for each of the configurations investigated. From these solutions, heat-rejection characteristics, such as individual fin and tube surface radiative efficiency and overall fin-tube effectiveness, can be obtained for each of the configurations.

In the analysis, it is assumed that energy input to the fin is composed of heat conduction along the fin from the fin base and incident radiation from the two base surfaces. In the case of the closed-sandwich configuration, additional incident radiation comes from the opposing fin surface. Radiant emission comes from both sides of the fin-tube panel to a surrounding environment of 0° R.

Several specific assumptions are used in the development of the fin heat-transfer relations for all the configurations considered:

(1) Incident radiation from external sources is negligible.

(2) The radiator surfaces act as blackbodies with incident and emitted radiation governed by Lambert's cosine law.

(3) Steady-state one-dimensional heat flow occurs in the fins with the fin base equal to the temperature of the tube outer surface.

(4) Fin and tube material properties are constant and evaluated at the fin-base temperature.

(5) The development of the fin and tube angle factors is based on an infinite longitudinal extent of fin and tube.

(6) Fin thickness is neglected in the determination of the view factor from the base surface to the fin.

(7) Temperature on the tube outer surface is constant circumferentially and longitudinally.

In all the configurations investigated, two dimensionless parameters are required to describe the heat transport adequately. These are the ratio of minimum fin half-length to tube outer radius L/R_o, which describes the effective cavity of the fin and tube, and the conductance parameter N_c, which describes the ratio of the radiating potential of the fin to its conducting potential. The conductance parameter is defined by the relation $N_c = \sigma l^2 T_b^3/kt$. For the configurations in figures 1(a), (c), and (d), $l = L$. An additional parameter is required to describe the variable tube side-wall thickness used in the closed-sandwich design (fig. 1(e)). This parameter is the ratio of the actual side-wall thickness of the tube to the thickness specified by the meteoroid protection criteria δ_s/δ_a. The curves presented in this report are plotted as functions of these parameters.

Central Fin and Tube

The analysis of reference 6 for the central fin and tube is based on the steady-state conservation of energy at any element of the fin. This would, in effect, balance energy input, which consists of heat conducted down the fin length plus incident radiation from the tubes, with energy output made up of conduction to a succeeding element and radiant emission to space. For the central fin and tube, the governing equation describing the fin temperature profile is, in dimensionless form (ref. 6),

$$\frac{d^2\theta}{dX^2} = N_c\left[\theta^4 - (F_{X-1} + F_{X-2})\right] \tag{1}$$

The view factors F_{X-1} and F_{X-2} are

$$F_{X-1} = \frac{1}{2}\left[1 - \frac{\sqrt{\left(\frac{R_o}{L} + X\right)^2 - \left(\frac{R_o}{L}\right)^2}}{\frac{R_o}{L} + X}\right]$$

$$F_{X-2} = \frac{1}{2}\left[1 - \frac{\sqrt{\left(\frac{R_o}{L} + 2 - X\right)^2 - \left(\frac{R_o}{L}\right)^2}}{\frac{R_o}{L} + 2 - X}\right]$$

Numerical techniques are required to solve the foregoing differential

equation for θ as a function of position X on the fin. This general procedure is used in the evaluation of all the differential equations for the geometries under consideration.

After the determination of the fin temperature profile, the net heat rejection from the fin is obtained by calculating the amount of heat flowing into the fin from the base surface. Defining Q_f as the net heat loss from one side of a fin of length L and comparing it with the ideal amount of energy that can be rejected from the surface yield the following dimensionless expression for the thermal efficiency of the fin:

$$\frac{\frac{Q_f}{Z}}{\sigma T_b^4 L} = -\frac{1}{N_c}\left(\frac{d\theta}{dX}\right)_{X=0} = \eta_f \tag{2}$$

where $(d\theta/dX)_{X=0}$ is obtained from the results of equation (1).

Inasmuch as the base-surface temperature is prescribed to be uniform, the net heat loss from the tube surface is the difference between the radiant emission and the incident energy from the fins and opposing base surface. Let Q_b be defined as the net heat loss from one-quarter of a tube outer surface. Comparison of the net heat rejection from the tube to the maximum emission possible from the periphery of the tube with no occulsion from the opposing tube and fin yields the expression (ref. 6)

$$\frac{\frac{Q_b}{Z}}{\sigma T_b^4 \frac{\pi R_o}{2}} = \frac{2}{\pi}\left[1 + \frac{L}{R_o}\int_0^1 (F_{X-1} + F_{X-2})(2 - \theta^4)dX\right] = \eta_b \tag{3}$$

The integral in equation (3) makes use of the fin temperature profile that was obtained from equation (1).

The following useful definition of overall fin-tube effectiveness is formulated from the definitions of fin efficiency in equation (2) and tube efficiency in equation (3):

$$\eta_R^* = \frac{Q_R}{\sigma T_b^4 ZL\left(1 + \frac{R_o}{L}\right)} = \frac{\eta_f}{1 + \frac{R_o}{L}} + \frac{\eta_b \frac{\pi}{2}\frac{R_o}{L}}{1 + \frac{R_o}{L}} \tag{4}$$

Equation (4) was derived for a quarter section of a tube and fin, but it is

identical to that for an entire fin-tube section of length $2(L + R_o)$ radiating from two sides.

The results of equations (2) and (3) for η_f and η_b are given and discussed in reference 6. The values of overall effectiveness η_R^* obtained from equation (4) are plotted against the ratio L/R_o for selected values of the conductance parameter in figure 2. Inspection of the curves shows the expected trend that overall effectiveness decreases as the ratio L/R_o increases. This is reasonable because, as the length of the fin increases with respect to a constant-diameter tube, the base surface plays a decreasingly important role in the percentage of heat rejected. Also, there is a reduction in the overall fin-tube heat loss as the conductance parameter increases. This is true because less heat is rejected from the fin as the temperature drop along the fin increases because of a higher conductance parameter. For a constant L/R_o and base temperature, the increased temperature drop would be brought about by a lower fin thermal conductivity or a thinner fin.

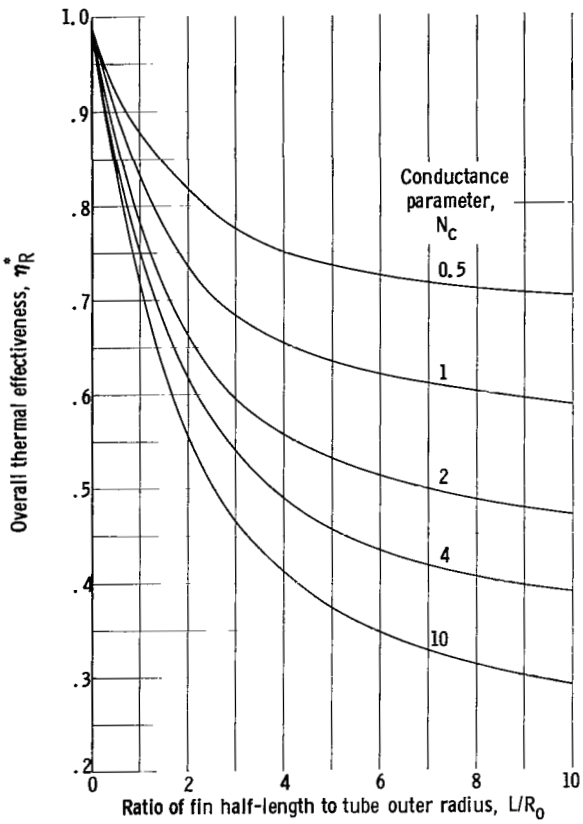

Figure 2. - Overall thermal effectiveness as function of ratio of fin half-length to tube outer radius for central-fin-and-tube configuration.

Open-Sandwich Fin and Tube Without Fillet

The open-sandwich configuration is practical from a fabrication viewpoint, because tubes might simply be attached to a flat plate that acts as the fin. In addition, the fin might serve as a meteoroid shield, and thus the weight of the radiator would be reduced. The round tube without a fillet, shown in figure 1(b), represents a limiting case of the open-sandwich configuration. The actual use of this configuration presents manufacturing difficulties because it would require line contact between tube and fin. In addition to mechanical problems, this design is not thermally sound; little, if any, cross-sectional area is available for conducting the heat to the fin from the tube. A large temperature difference would exist, and thus the thermal effectiveness of the system would be reduced.

The analysis of this configuration given in reference 10 contains errors in the angle factors. Introduction of the proper expressions to the energy equation for an element of the fin is shown in the appendix. Derivations of the governing equations for the determination of fin temperature profiles, base-surface effectiveness, fin effectiveness, and overall effectiveness are also given in the appendix.

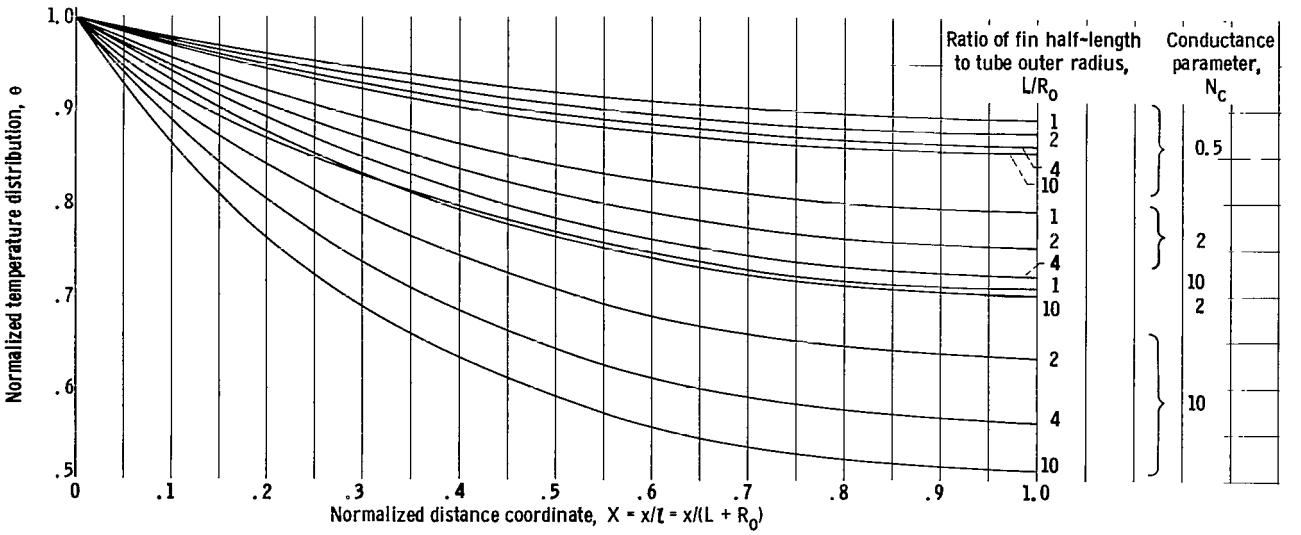

Figure 3. - Fin temperature profile for open-sandwich fin tube without fillet.

Curves for temperature along the fin for various values of the conductance parameter N_c and the ratio L/R_o are shown in figure 3. It is observed from these curves that the fin temperature decreases as the ratio L/R_o increases

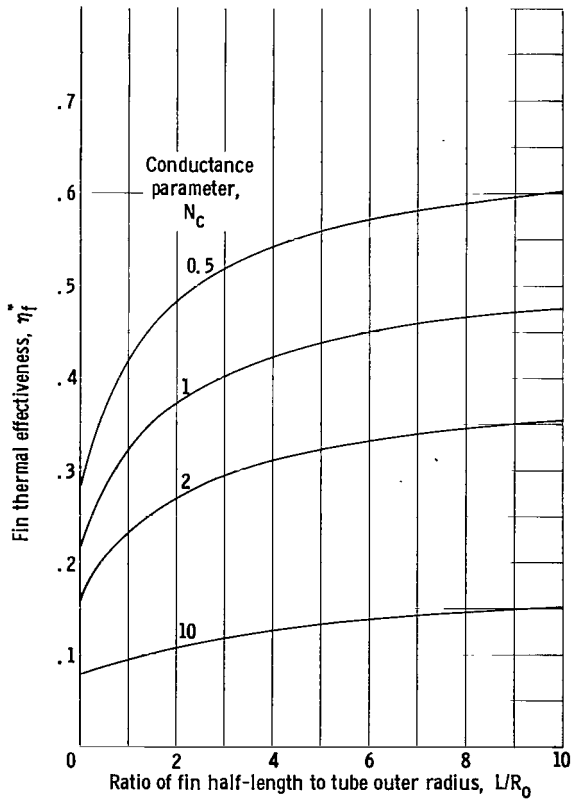

Figure 4. - Fin effectiveness as function of ratio of fin half-length to tube outer radius for open-sandwich fin-tube configuration without fillet.

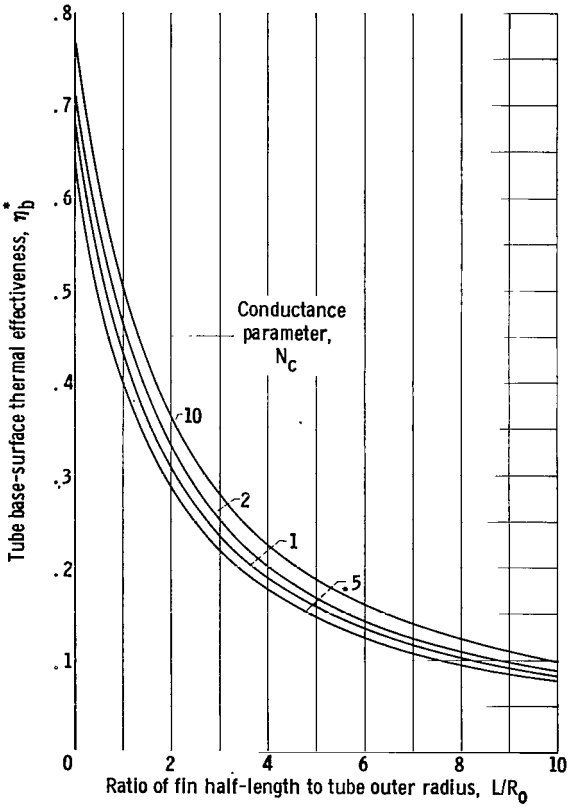

Figure 5. - Tube base-surface thermal effectiveness as function of ratio of fin half-length to tube outer radius for open-sandwich fin-tube configuration without fillet.

for a constant N_c. This is reasonable if the tube is considered to play a less significant role in radiating heat to the fin as L/R_o increases. A decrease in fin temperature also exists as N_c is increased for constant L/R_o. This is true because an increasing N_c is just a decreasing thermal conductance of the fin material that increases the resistance to heat flow and, thus, requires a greater potential to reject the same amount of heat. Another interesting aspect of this figure is that, as the conductance parameter gets larger, the effects of the tube become more noticeable. In particular, the temperature at the middle of the fin is lower and is thus affected to a greater extent by any incident radiation from the tube.

Figure 4 shows curves for fin thermal effectiveness against the ratio L/R_o for a selected variation in conductance parameter. These results show the usual trend of decreasing fin effectiveness with increasing N_c and decreasing L/R_o. An interesting feature of this configuration occurs when L/R_o equals zero. At this point, the tubes touch, but a fin $2R_o$ long still remains. Thus, the fin effectiveness does not equal zero at $L/R_o = 0$, as was the case for the central-fin geometry. As the conductance parameter approaches zero, the fin effectiveness becomes large but not equal to the limiting value of 1. This limit is only attained with the additional stipulation that L/R_o must equal infinity.

The base-surface effectiveness, shown in figure 5, approaches zero as L/R_o goes to infinity and approaches finite values as L/R_o approaches zero, where the minimum effectiveness would be equal to 50 percent for an N_c of zero.

The overall fin-tube thermal effectiveness can then be obtained from the expression

$$\eta_R^* = \int_0^1 (F_{X-1} + F_{X-2})\left(1 - \frac{1}{2}\theta^4\right)dX - \frac{1}{N_c}\left(\frac{d\theta}{dX}\right)_{X=0} \tag{5}$$

which is derived in the appendix. The overall fin-tube effectiveness obtained from equation (5) is plotted against L/R_o for selected values of N_c in figure 6. This curve shows the expected result that the overall effectiveness approaches the fin efficiency of a flat plate when L/R_o becomes very large. The total effectiveness does not equal unity as L/R_o approaches zero because of the presence of the nonisothermal fins of length $2R_o$.

Open-Sandwich Fin and Tube with Fillet

The open-sandwich configurations with fillets are shown in figures 1(c) and (d). The fin-tube arrangement of figure 1(c) is constructed by the addition of a fillet to the configuration of figure 1(b), whereas in the configuration of figure 1(d) it is assumed that the portion of the fin below the tube also

acts as meteoroid armor, so that the required tube wall thickness is reduced at this point.

These geometries would be reasonable designs because of good heat-transfer properties and easy fabrication. Fabrication would be simplified because fillets would be used, and the thermal problem of transferring heat from the tube wall to the fin would be alleviated by the increased cross-sectional area introduced by the weld material. In the analysis it is assumed that the actual fin starts at the fillet and not at the tube centerline, as was the situation without a fillet. This assumption is reasonable because most fillet materials used will be of high thermal conductivity and applied in a manner that will limit the contact resistance at the bond.

On the basis of a thermal analysis, both schemes can be evaluated in an identical manner because fin thickness is neglected in the radiant interchange, and temperature drops in the tube wall are not included. The thermal analysis of the fin resulted in the following differential equation:

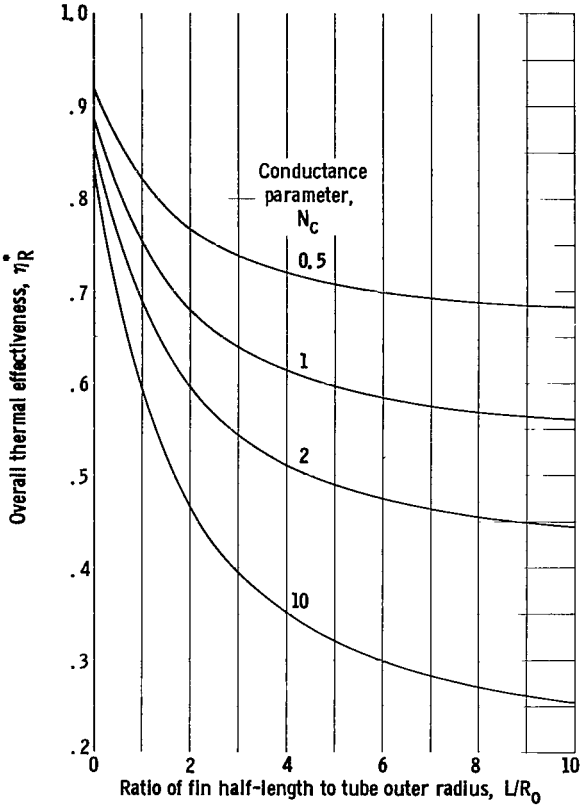

Figure 6. - Overall thermal effectiveness as function of ratio of fin half-length to tube outer radius for open-sandwich fin-tube configuration without fillet.

$$\frac{d^2\theta}{dX^2} = N_c\left[\theta_X^4 - \frac{1}{2}\left(F_{X-2} + F_{X-1}\right)\right] \tag{6}$$

where the view factors F_{X-1} and F_{X-2} are derived with the same principal used for the open-sandwich fin and tube without a fillet described in the appendix. These results are

$$F_{X-1} = \frac{1}{1 + \left(1 + X\,\frac{L}{R_o}\right)^2}$$

$$F_{X-2} = \frac{1}{1 + \left[1 + (2 - X)\,\frac{L}{R_o}\right]^2}$$

The solution of equation (6) yields the temperature profile of the fin. Typical solutions are given in figure 7 for variations in conductance parameter

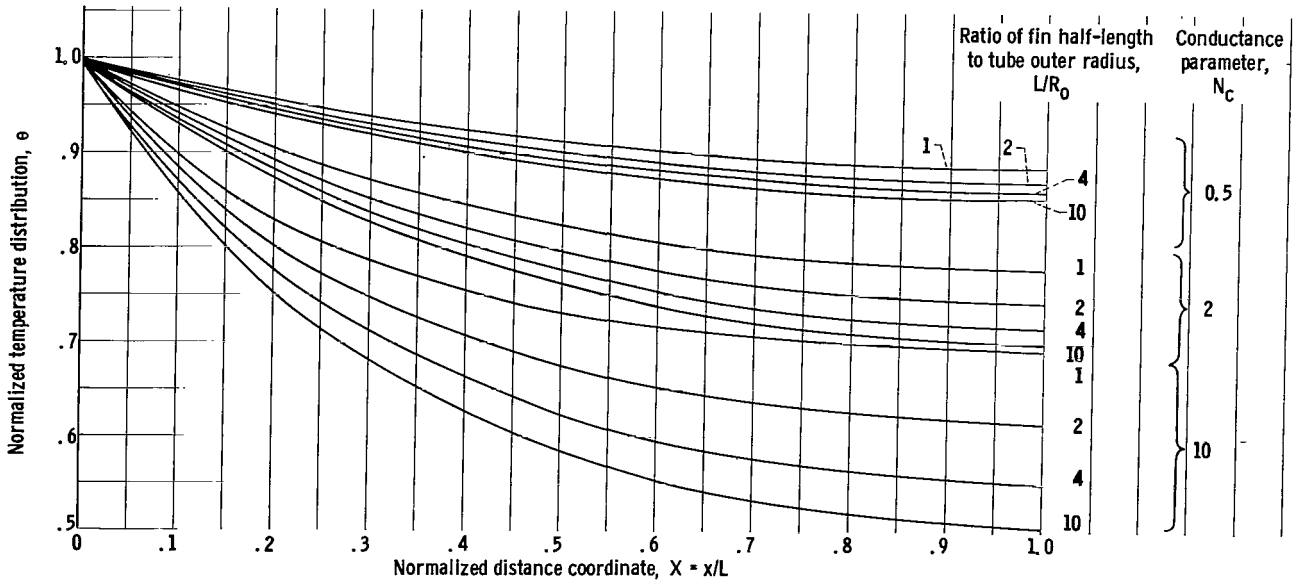

Figure 7. - Fin temperature profile for open-sandwich fin-tube configuration with fillet.

and L/R_o. The same comments can be made with regard to trends for this configuration as were given for the configuration without a fillet.

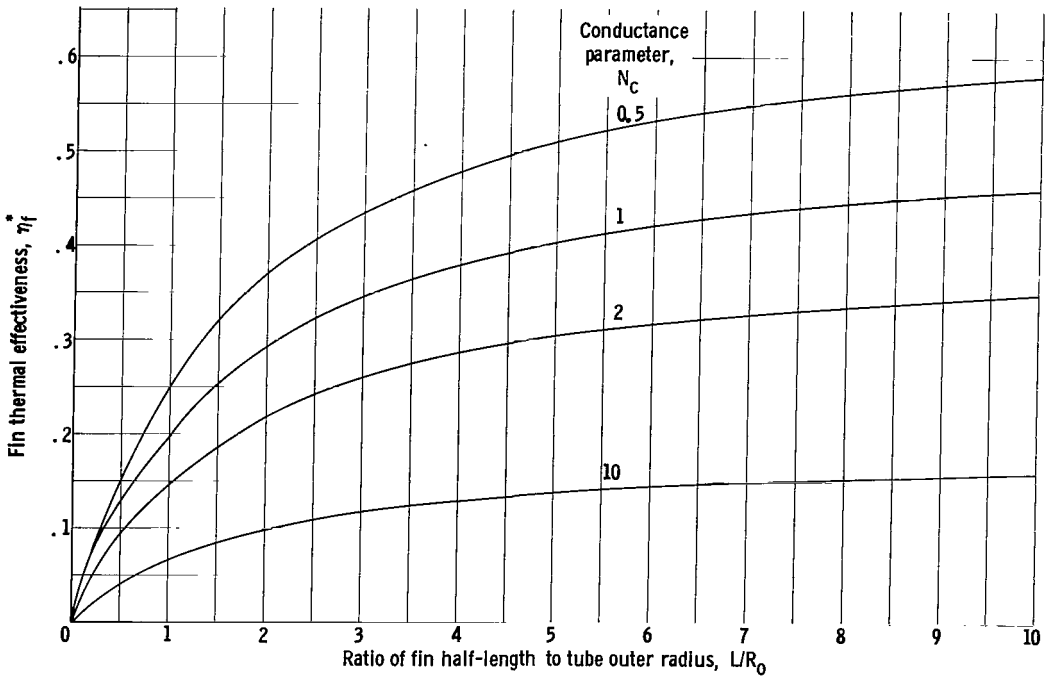

Figure 8. - Fin thermal effectiveness as function of ratio of fin half-length to tube outer radius for open-sandwich fin-tube configuration with fillet.

These results are then used to obtain the effectiveness of the fin and of the base surface by using the following equations:

$$\eta_f^* = \frac{2Q_f}{4\sigma L T_b^4 \left(1 + \frac{R_o}{L}\right) Z} = -\frac{1}{N_c} \frac{1}{1 + \frac{R_o}{L}} \left(\frac{d\theta}{dX}\right)_{X=0} \tag{7}$$

$$\eta_b^* = \frac{2Q_b}{4\sigma L T_b^4 \left(1 + \frac{R_o}{L}\right) Z} = \frac{1}{1 + \frac{L}{R_o}} \left[1 + \frac{L}{R_o} \int_0^1 (F_{X-1} + F_{X-2}) \left(\frac{3}{2} - \frac{1}{2}\theta^4\right) dX\right] \tag{8}$$

where Q_f and Q_b are defined as the net energy rejected from the fin and base surface, respectively, of a span of length $L + R_o$ radiating from both sides. The results of equation (7) are shown in figure 8 and those of

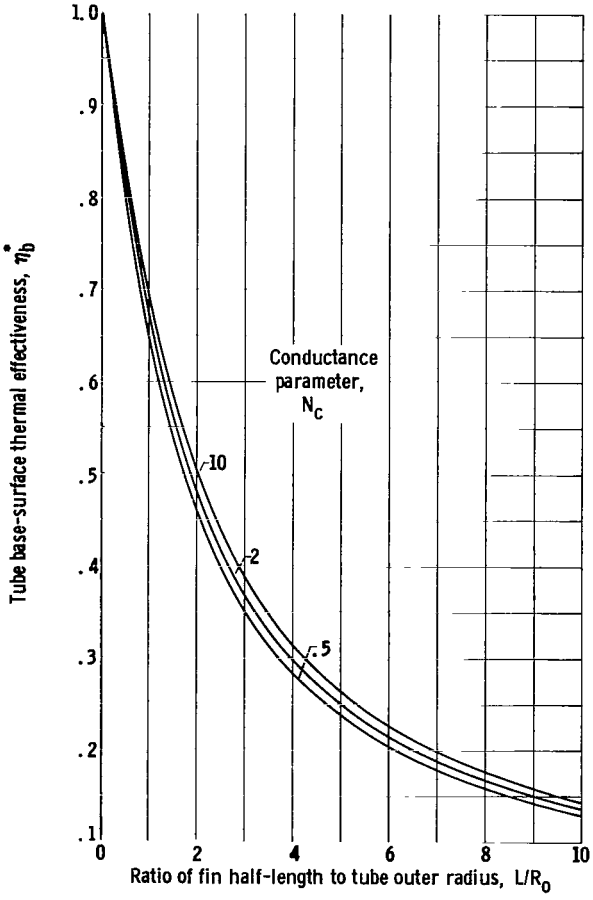

Figure 9. - Tube base-surface thermal effectiveness as function of ratio of fin half-length to tube outer radius for open-sandwich fin-tube configuration with fillet.

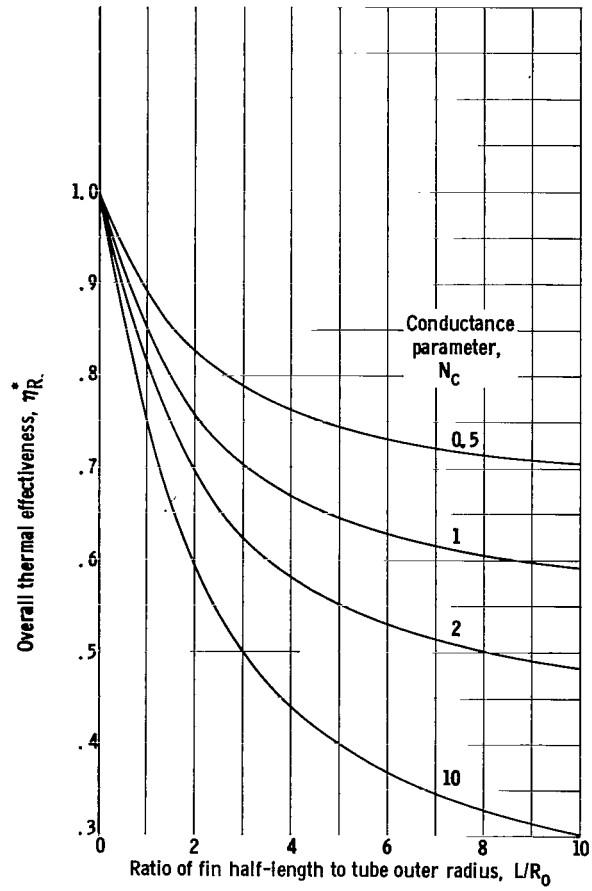

Figure 10. - Overall thermal effectiveness as function of ratio of fin half-length to tube outer radius for open-sandwich fin-tube configuration with fillet.

equation (8) in figure 9. The summation of these two expressions for effectiveness yields the overall fin-tube effectiveness:

$$\eta_R^* = \frac{1}{1 + \frac{R_o}{L}} \left[\frac{R_o}{L} - \frac{1}{N_c} \left(\frac{d\theta}{dX} \right)_{X=0} + \int_0^1 (F_{X-1} + F_{X-2}) \left(\frac{3}{2} - \frac{1}{2} \theta^4 \right) dX \right] \tag{9}$$

The results of equation (9) are plotted against L/R_o for selected values of N_c in figure 10, which shows that the overall fin-tube thermal effectiveness decreases as the conductance parameter or the ratio L/R_o increases.

Closed-Sandwich Fin and Tube with Variable Side-Wall Thickness

The closed-sandwich design shown in figure 1(e) has a practical application in its ability to act as a bumper screen that will afford protection against meteoroids on both faces of the radiator tube. The configuration shown is a general case because it allows for a reduction in the tube side-wall thickness since the fin will act as a bumper. In the geometries under investigation, it is assumed that the tube can be approximated by a square tube as a result of the addition of fillets required to improve heat transfer and structural reliability.

The analysis for the fin temperature profile of this configuration is more complex than either the central fin or the open-sandwich analysis because two nonisothermal surfaces are present instead of one. The development of the fin energy equation (ref. 12) is similar to that of the previous cases with the exception that no internal emission is transferred to space. This results in an integrodifferential equation in which the integral is introduced as a result of the emission from one internal fin surface to an element of another. This equation in general form is

$$\frac{1}{N_c} \left(\frac{d^2\theta}{dX^2} \right) = 2\theta_X^4 - 2 \left(\frac{R_o}{l} \right)^2 \int_0^1 \theta_Y^4 \, dY \left\{ \frac{1}{\left[(Y - X)^2 + 4 \left(\frac{R_o}{l} \right)^2 \right]^{3/2}} + \frac{1}{\left[(2 - Y - X)^2 + 4 \left(\frac{R_o}{l} \right)^2 \right]^{3/2}} \right\} - 1 + \frac{1}{2} \left\{ \frac{X}{\left[X^2 + 4 \left(\frac{R_o}{l} \right)^2 \right]^{1/2}} + \frac{2 - X}{\left[(2 - X)^2 + 4 \left(\frac{R_o}{l} \right)^2 \right]^{1/2}} \right\} \tag{10}$$

where the fin position parameters X and Y are $X = x/l$ and $Y = y/l$, and the actual fin length is

$$l = L + \left(1 - \frac{\delta_s}{\delta_a}\right)\delta_a$$

The parameter δ_s/δ_a is introduced to define the fraction of the armor thickness δ_a retained on the enclosed side of the tube. This parameter will be varied from 0 to 1 for each value of N_c and L/R_o. The resultant tempera-

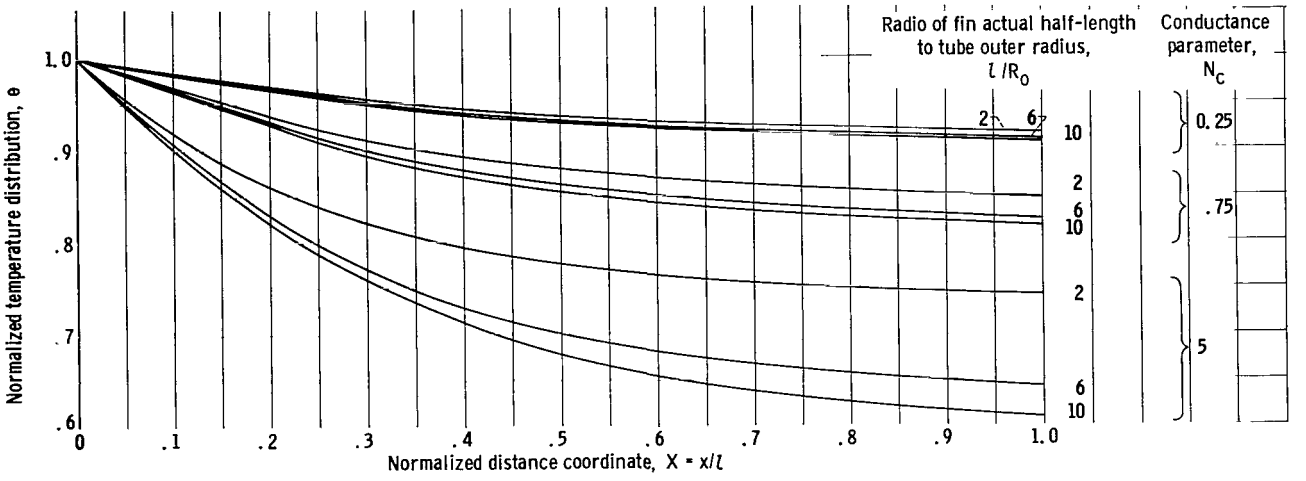

Figure 11. - Fin temperature profile for closed-sandwich configuration.

ture profiles obtained from the solution of equation (10) are shown plotted in figure 11 as a function of x/l for selected values of N_c and the ratio R_o/l.

When the temperature profile of the fin is obtained, the fin and base-surface effectiveness may be determined. Reference 12 points out that the heat transfer from the fin cannot be calculated by determining the amount of heat conducted into the fin from the base surface at $X = 0$. Internal radiation is also a contributor since, in effect, it acts like the heat conduction along the fin and thus forms parallel heat-flow paths. The fin heat rejection must then be calculated from the temperature profile obtained from equation (10). Comparing this heat rejection to the maximum that can be rejected from both sides of an isothermal fin-tube geometry of length $2(l + h)$ yields the fin-effectiveness expression

$$\eta_f^* = \frac{2Q_f}{4\sigma Z l T_b^4\left(1 + \frac{h}{l}\right)} = \frac{1}{1 + \frac{h}{l}} \int_0^1 \theta^4 \, dX \qquad (11a)$$

where

$$\frac{h}{l} = \frac{R_o - \left(1 - \frac{\delta_s}{\delta_a}\right)\delta_a}{L + \left(1 - \frac{\delta_s}{\delta_a}\right)\delta_a} \tag{11b}$$

and θ is a function of X for specific values of δ_s/δ_a, L/R_o, and N_c.

The base-surface effectiveness can be calculated by using equation (12):

$$\eta_b^* = \frac{2Q_b}{4\sigma Z l T_b^4\left(1 + \frac{h}{l}\right)} = \frac{1}{1 + \frac{l}{h}} \tag{12}$$

where l/h is defined in terms of R_o, L, δ_a, and δ_s in equation (11b). The overall effectiveness is then obtained by adding the results of equations (11a) and (12). This expression is

$$\eta_R^* = \frac{1}{1 + \frac{l}{h}}\left(1 + \frac{l}{h}\int_0^1 \theta^4\, dX\right) \tag{13}$$

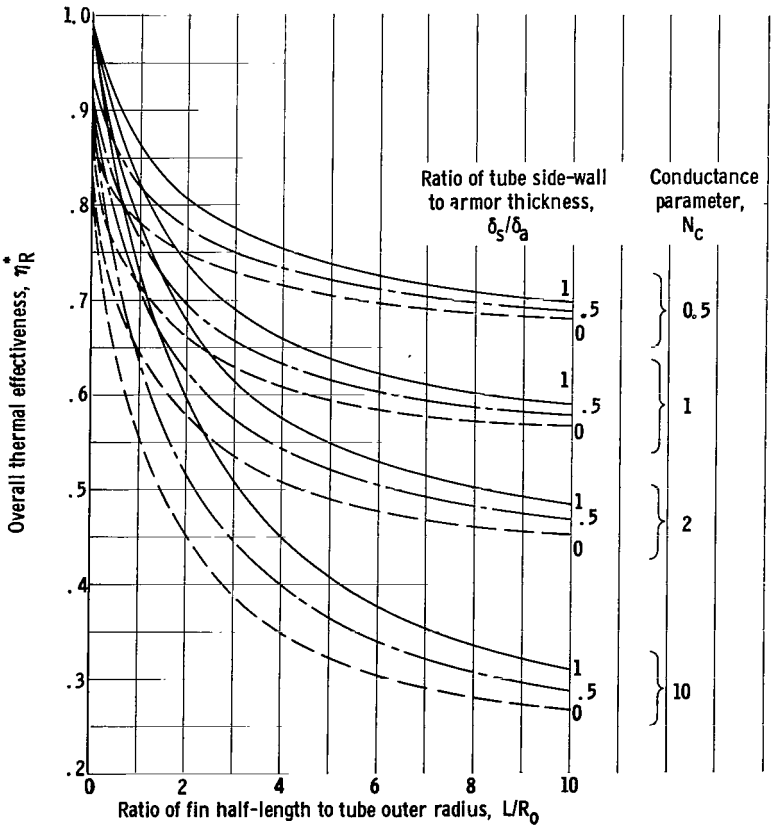

Figure 12. - Overall thermal effectiveness as function of ratio of fin half-length to tube outer radius for closed-sandwich fin-tube configuration. Tube vulnerable area based on round tube or on tube projected area.

In equation (13) for the overall fin-tube effectiveness, it is seen that the tube wall thickness δ_a must be known in order to obtain solutions for cases when δ_s/δ_a is something other than 1. The actual value of δ_a can be obtained for any choice of L/R_o and N_c when tube inside diameter D_i, tube liner thickness δ_c, power, temperature, materials, meteoroid protection criteria, and definition of radiator tube vulnerable area are specified. The unique value of δ_a obtained for each choice of L/R_o and N_c was calculated for $\delta_s/\delta_a = 1$ and kept constant as δ_s/δ_a was varied.

Figure 12 is a plot of

overall fin-tube effectiveness η_R^* against L/R_o and N_c for a 1-megawatt powerplant radiating at 1700° R with the tube vulnerable area defined as that of a round tube ($A_v = 2\pi ZR_o$) or as twice the tube projected area ($A_v = 4ZR_o$). Negligible difference existed between the two cases because the change in thickness δ_a obtained from the optimization was small. Inspection of the curves shown in figure 12 reveals that, for any fixed value of L/R_o and N_c, the overall fin-tube thermal effectiveness decreases as δ_s/δ_a decreases. This is reasonable because, as δ_s/δ_a decreases, the amount of isothermal base surface decreases. The fin-tube effectiveness is also reduced by increasing the conductance parameter or by increasing L/R_o.

Comparison of Results

Comparisons of the heat-rejection results obtained for the fin-tube configurations under investigation are shown in figures 12 and 13. In figure 12 thermal effectiveness is plotted against L/R_o for the closed-sandwich configuration; in figure 13 results are given for four configurations, the central fin, the open sandwich without a fillet, the open sandwich with a fillet, and the closed sandwich ($\delta_s/\delta_a = 1$). For a typical choice of N_c equal to 1, a variation of less than 1 percent exists in the overall fin-tube thermal effectiveness of the central fin, the open sandwich with a fillet, and the closed sandwich with no bumper effect by the fin ($\delta_s/\delta_a = 1$). This variation increases to 7 percent for a conductance parameter of 10. The remaining configurations, that is, the open sandwich without a fillet and the variable-side-wall closed sandwich, exhibit lower values of thermal effectiveness than those of the previously mentioned geometries for the same values of L/R_o and N_c.

Although the configurations can all be compared for the same values of conductance parameter and L/R_o, this does not necessarily imply they all have the same fin length. Differences in fin length could be brought about by variations in δ_a or by the basic configuration itself. As for the open-sandwich configuration without a fillet and the variable side-wall closed-sandwich configurations, they would then have longer and thicker fins, as prescribed by the conductance parameter.

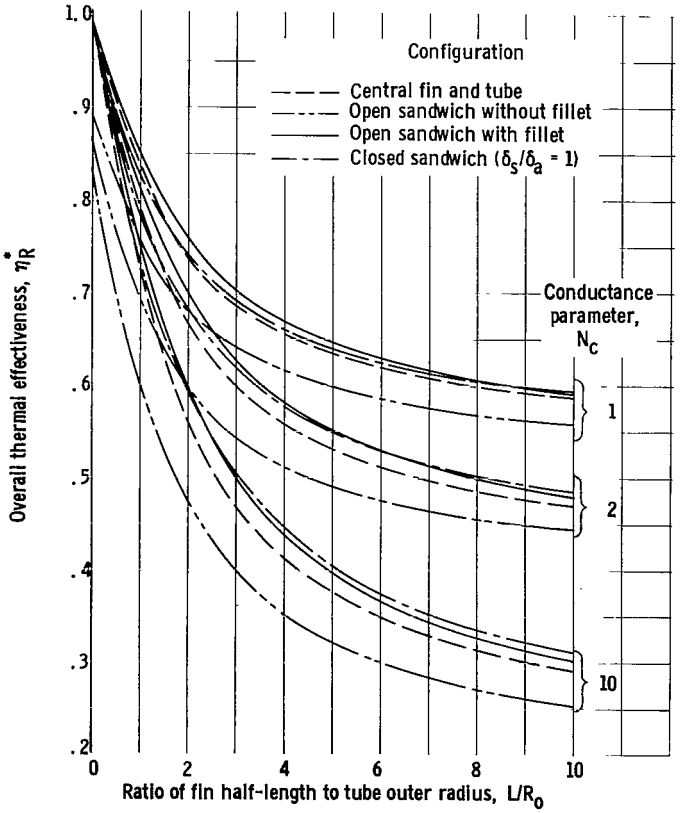

Figure 13. - Overall thermal effectiveness as function of ratio of fin half-length to tube outer radius for four configurations.

RADIATOR WEIGHT ANALYSIS

The foregoing presentation of results has been focused on the heat-transfer characteristics of the specific configurations under investigation. The proper choice of a configuration, however, cannot be made on the basis of heat rejection only. Radiator weight must be included. Because of additional variables such as tube internal diameter, meteoroid armor thickness, radiator materials, radiator temperature level, and system power level, weight optimizations can only be made for specific cases. Input information required from the heat-rejection analysis consists of the overall radiator effectiveness as a function of N_c, L/R_o, and δ_s/δ_a.

Assumptions

The specific assumptions adopted in the formulation of the relations for radiator panel weight are

(1) All tubes contain a thin-walled liner of columbium alloy to contain the fluid. The liner thickness was made a function of inside tube diameter given by the arbitrary schedule $\delta_c = 0.04\ D_i$.

(2) The meteoroid protection criterion used in this analysis is that of reference 13.

(3) The radiator materials consist of beryllium fins and tube armor and columbium tube liners.

(4) A typical inside tube diameter of 3/4 inch was used for all the geometries investigated.

(5) Pressure drop in the tubes and weight of the liquid and vapor headers were not considered.

In essence, this last assumption permits the analysis of a single tube and fin without regard to number of tubes and subsequent individual tube length.

The heat-rejection capabilities per unit weight are presented here for a typical advanced space power application. The powerplant consists of a 1-megawatt-output Rankine power-generation system operating at a condenser temperature of 1700° R with an overall cycle efficiency of 15 percent. For simplicity it is assumed that, for a specified powerplant output and overall cycle efficiency, the following expression is valid for obtaining the required radiator heat-rejection load:

$$Q_R = 3.413 \times 10^6\ P_e \left(\frac{1}{\eta_c} - 1 \right) \tag{14}$$

Meteoroid Protection

The meteoroid protection criteria given in reference 13 are based on a comprehensive and definitive appraisal of the data and theories available concerning the meteoroid penetration phenomenon. According to reference 13, the resultant equation for the armor thickness δ_a is given by

$$\delta_a = 2a\left(\frac{\rho_p 62.45}{\rho_a}\right)^{1/2}\left(\frac{\overline{V}_p}{c_a}\right)^{2/3}\left(\frac{6.747\times10^{-5}}{\rho_p}\right)^{1/3}\left[\frac{\alpha A_v \tau}{-\ln P(0)}\right]^{1/3\beta}\left(\frac{1}{\beta+1}\right)^{1/3\beta} \tag{15}$$

where a is 1.75, $\overline{V}_p$ is 98,400 feet per second, α is 0.53×10^{-10} gram$^{\beta}$ per square foot per day, β is 1.34, and ρ_p is 0.44 gram per cubic centimeter. A mission time τ of 500 days was chosen for the comparison with a probability of no punctures $P(0)$ of 0.998.

The radiator vulnerable area A_v was taken as the total outer surface area of a round tube for all five radiator configurations investigated:

$$A_v = 2\pi R_o Z = \frac{\pi Q_R}{2\sigma T_b^4\left(1+\frac{L}{R_o}\right)\eta_R^*} \tag{16}$$

The closed-sandwich fin-tube configuration is also treated by using a definition of vulnerable area which assumes that both fins act as bumper screens to meteoroids and that only the projected area of the tube outside diameter is considered:

$$A_v = 4R_o Z = \frac{Q_R}{\sigma T_b^4\left(1+\frac{L}{R_o}\right)\eta_R^*} \tag{17}$$

The closed-sandwich configuration is compared in this manner to show the possible upper limit of heat rejection per unit weight.

Weight Ratio

Once the tube armor thickness δ_a has been obtained, the heat rejection per unit weight of a fin-tube radiator can be calculated from the expression

$$\frac{Q}{W} = \frac{\frac{Q}{Z}}{\frac{W}{Z}} \tag{18}$$

where the heat rejection per unit length of tube is given by

$$\frac{Q}{Z} = 2D_o\left(1 + \frac{L}{R_o}\right)\eta_R^*\sigma T_b^4 \tag{19}$$

and values of η_R^* for the various configurations are obtained from the heat-rejection analyses. The fin and tube weight per unit length of tube can be calculated by summing the weight of the fins, the tube liner, and the tube armor. For the fin and tube geometries considered in this comparison, the weights per unit length are as follows:

Central fin and tube (fig. 1(a)):

$$\frac{W}{Z} = \frac{4\rho_f\sigma T_b^3}{kN_c}\left(\frac{L}{R_o}\right)^3(R_i + \delta_c + \delta_a)^3 + \rho_c\pi\delta_c(D_i + \delta_c) + \rho_a\pi\delta_a(D_i + 2\delta_c + \delta_a) \tag{20}$$

Open-sandwich fin and tube without a fillet (fig. 1(b)):

$$\frac{W}{Z} = \frac{4\rho_f\sigma T_b^3}{kN_c}\left(1 + \frac{L}{R_o}\right)^3(R_i + \delta_c + \delta_a)^3 + \rho_c\pi\delta_c(D_i + \delta_c) + \rho_a\pi\delta_a(D_i + 2\delta_c + \delta_a) \tag{21}$$

Open-sandwich fin and tube with a fillet (fin meteoroid protection neglected) (fig. 1(c)):

$$\frac{W}{Z} = \frac{4\rho_f\sigma T_b^3}{kN_c}\left[\left(\frac{L}{R_o}\right)^3 + \left(\frac{L}{R_o}\right)^2\right](R_i + \delta_c + \delta_a)^3 + \rho_c\pi\delta_c(D_i + \delta_c) + \rho_a\left[\left(2 + \frac{\pi}{2}\right)(R_i + \delta_c + \delta_a)^2 - \pi(R_i + \delta_c)^2\right] \tag{22}$$

Open-sandwich fin and tube with a fillet (fin meteoroid protection assumed) (fig. 1(d)):

$$\frac{W}{Z} = \frac{4\rho_f\sigma T_b^3}{kN_c}\left(\frac{L}{R_o}\right)^3(R_i + \delta_c + \delta_a)^3 + \rho_c\pi\delta_c(D_i + \delta_c) + \rho_a\left[\left(2 + \frac{\pi}{2}\right)(R_i + \delta_c + \delta_a)^2 - \pi(R_i + \delta_c)^2\right] \tag{23}$$

Closed-sandwich fin and tube with variable side wall (fig. 1(e)):

$$\frac{W}{Z} = \frac{4\rho_f \sigma T_b^3}{kN_c}\left[\frac{L}{R_o} + \left(1 - \frac{\delta_s}{\delta_a}\right)\frac{\delta_a}{R_o}\right]^3 (R_i + \delta_c + \delta_a)^3 + \rho_c \pi \delta_c (D_i + \delta_c)$$

$$+ \rho_a \left\{4R_o\left[R_i + \delta_c + \left(\frac{\delta_s}{\delta_a}\right)\delta_a\right] - \pi(R_i + \delta_c)^2\right\} \qquad (24)$$

CALCULATIONS AND RESULTS

Calculations employing the results of the thermal analysis for the five configurations investigated (eqs. (4), (5), (9), or (13)) along with the armor thickness equation (15) and the vulnerable area expressions (16) and (17) yield the required tube armor thickness δ_a for each configuration. Once δ_a has been obtained, the radiator weights can be calculated for the five geometries of figure 1 by using equations (20) to (24). Equation (18) can then be used to obtain the heat rejected per unit weight of a fin-tube radiator for any specific choice of

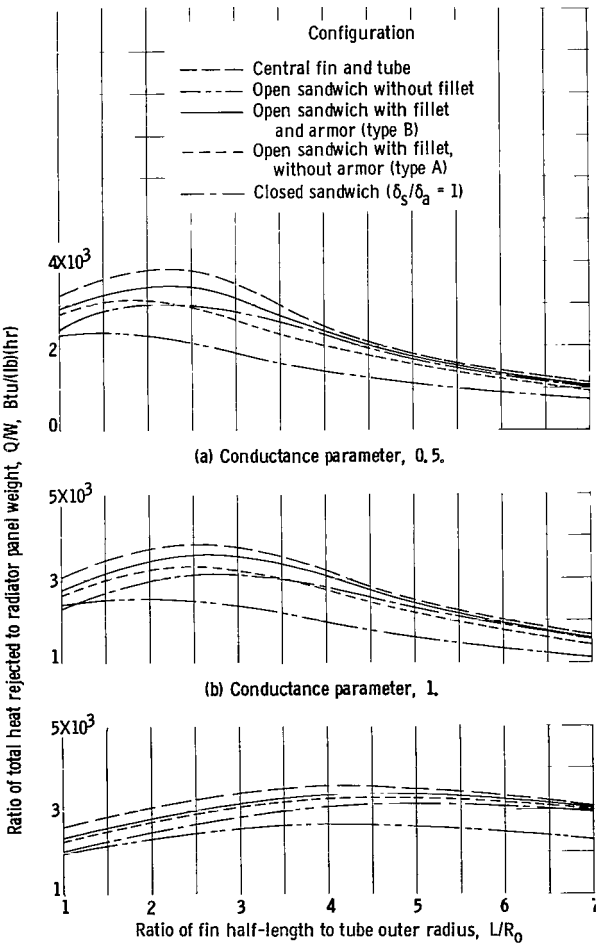

Figure 14. - Comparison of ratio of heat rejected to fin-tube weight for various conductance parameters and configurations. Tube vulnerable area based on round tube.

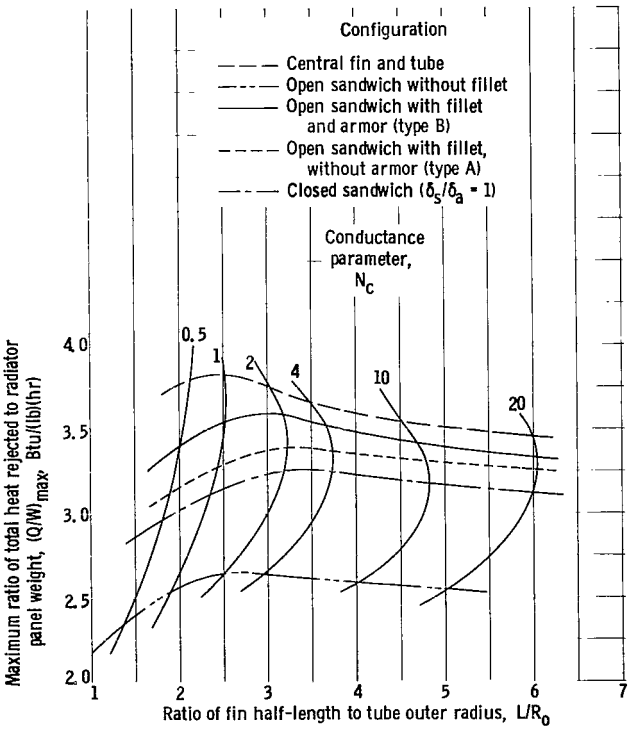

Figure 15. - Comparison of maximum ratio of heat rejected to fin-tube weight for various configurations. Power output, 1 megawatt; tube inside diameter, 3/4 inch; radiator temperature, 1700° R; fin and armor material, beryllium.

N_c and L/R_o, and in the case of the closed sandwich, δ_s/δ_a.

Figure 14 illustrates the variation of the ratio of total heat rejected to radiator panel weight with the ratio L/R_o and the conductance parameter N_c for the five geometries with vulnerable area based on the round tube with full side-wall thickness. The central-fin configuration maintains the maximum Q/W regardless of the choice of L/R_o or N_c. Each curve peaks at a single value of L/R_o, and the value depends on the choice of N_c. All the values of Q/W tend to approach each other as L/R_o becomes large for each value of N_c. The difference in Q/W between the most desirable configuration (central fin and tube) and the least desirable (open sandwich without a fillet) at a typical value of N_c of 1 is 35 percent at their respective maximum points.

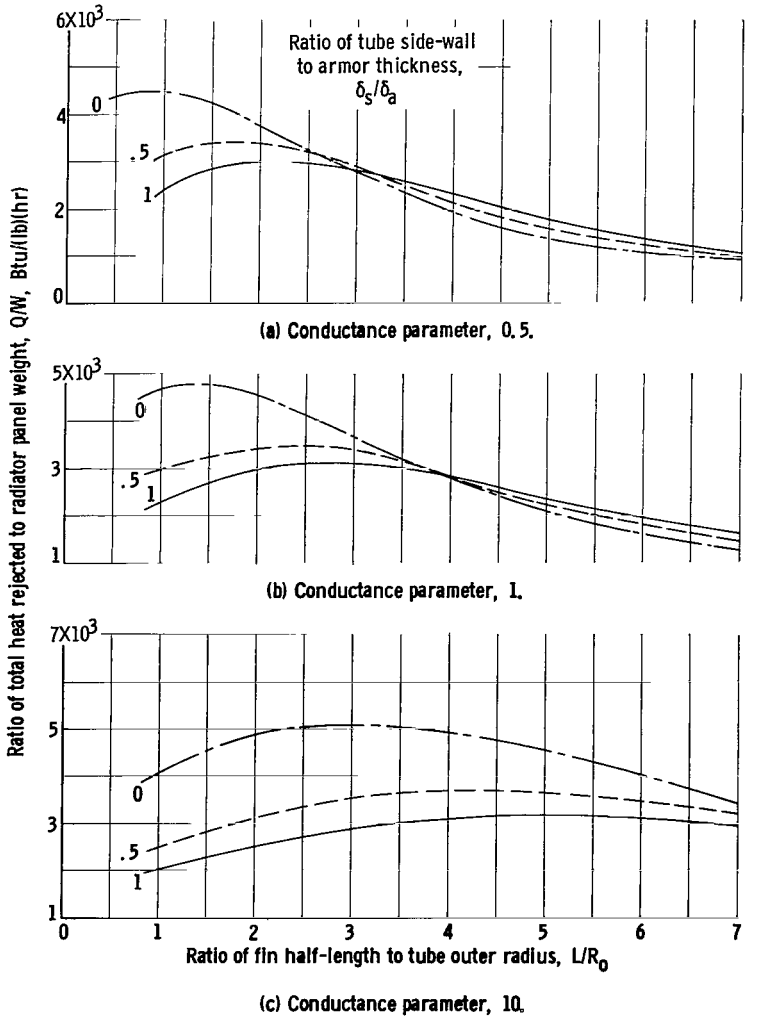

Figure 16. - Comparison of ratio of heat rejected to fin-tube weight for various conductance parameters. Closed-sandwich configuration. Tube vulnerable area based on round tube. Power output, 1 megawatt; tube inside diameter, 3/4 inch; radiator temperature, 1700° R; fin and armor material, beryllium.

Curves of maximum values of Q/W against L/R_o for the values of N_c considered are shown in figure 15 for the five configurations previously mentioned. This set of curves substantiates the fact that the central fin and tube maintains its superiority over the entire practical range of N_c investigated. Each of the curves peaks at a different value of N_c, the central fin peaking at an N_c of 1 and the remaining geometries at higher values. This comparison clearly points out that the open-sandwich configuration without a fillet is not a good choice from the standpoint of heat rejection per unit weight.

Figure 16 shows Q/W plotted against L/R_o for three values of N_c for the closed-sandwich configuration with vulnerable area based on the round tube with variable side-wall thickness. The curves show that a substantial weight saving is achieved by reducing the tube side-wall thickness for the three representative choices of N_c at the L/R_o corresponding to maximum Q/W. An

interesting aspect of the curves of figure 16 is that, below an L/R_o of 3 for an N_c of 0.5, the curve for a δ_s/δ_a of 0 has the highest Q/W, but at values of L/R_o greater than 3, a crossover occurs for a δ_s/δ_a of 1.0 and yields the greater value of Q/W. This crossover results from the variation in fin length of the three configurations, which for a constant value of N_c results in a corresponding variation in fin thickness t. Thus, as L/R_o increases, the fin becomes increasingly important and results in increased weight as δ_s/δ_a values approach 1. Crossover can occur at larger values of L/R_o as the conductance parameter is increased.

Curves of the maximum values of Q/W against L/R_o for the three closed-sandwich configurations along with the central-fin-and-tube configuration are shown in figure 17. Maximum Q/W for the closed-sandwich configurations occurs at much larger values of N_c than that of the central fin and tube. For the limiting case of δ_s/δ_a of 0, the optimum value of N_c is about 10. It is also observed that a value of δ_s/δ_a less than 0.5 must be used in order to better the results of the conventional central fin and tube.

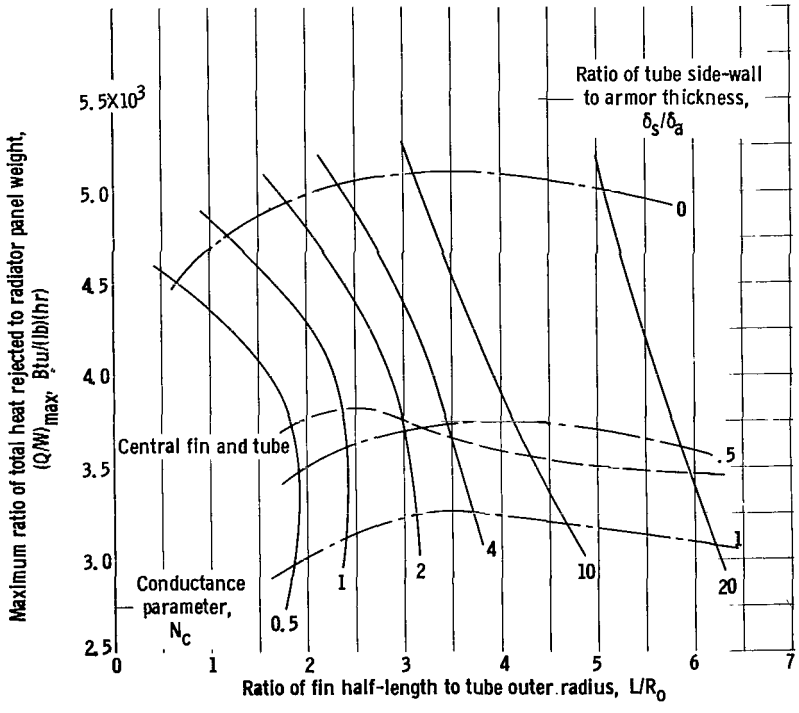

Figure 17. - Comparison of maximum ratio of heat rejected to fin-tube weight for closed-sandwich configuration. Tube vulnerable area based on round tube.

The closed-sandwich configurations with variable side walls were recalculated with twice the tube projected area obtained for δ_s/δ_a of 1 taken as the vulnerable area for meteoroid protection. Figures 18 and 19 show these results plotted in the same manner as the results of the previous closed-sandwich fin-tube configurations. A maximum weight saving of 7 percent at maximum Q/W resulted with the revised definition of tube vulnerable area.

Comparison of all the geometries investigated indicates that a maximum possible weight saving of 38 percent could be realized if the closed-sandwich fin-tube configuration with a δ_s/δ_a of 0 and tube vulnerable area based on the projected area could be used instead of the conventional central-fin-and-tube configuration. This advantage is reduced to 7 percent if a side-wall-thickness ratio δ_s/δ_a of 0.5 is used, and hence shows the desirability of further investigation of the bumper-screen concept in the design of minimum-weight space radiators.

The results and comparison indicated must be qualified, however, in that the effects of pressure drop, temperature drop through the tube armor, and

vapor and liquid headers were not considered in the weight optimization.

RADIATOR GEOMETRY

The importance of minimizing radiator fin and tube weight has been amply acknowledged in the available literature and numerous efforts have been undertaken to this end. In many cases it is also of considerable interest to determine the required geometry of the radiator panel (i.e., planform area and fin thickness) in order to facilitate such factors as fabrication or proper integration of the radiator and the space vehicle. The fin-tube configurations analyzed in this study are also compared on this basis for the 1-megawatt powerplant example.

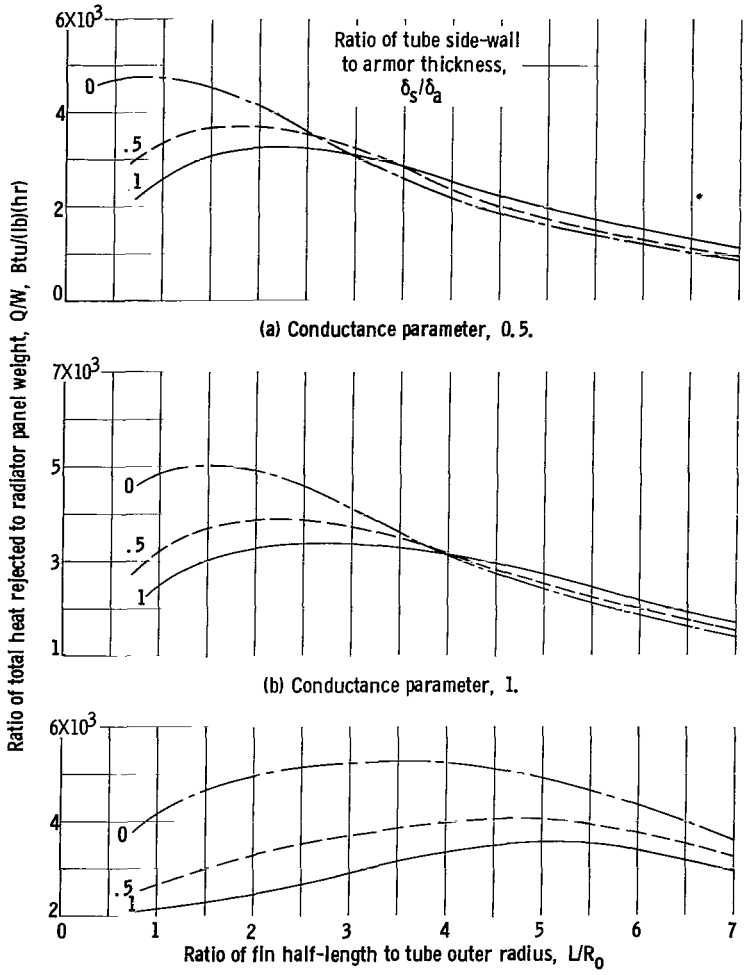

(a) Conductance parameter, 0.5.

(b) Conductance parameter, 1.

(c) Conductance parameter, 10.

Figure 18. - Comparison of ratio of heat rejected to fin-tube weight for various conductance parameters. Closed-sandwich configuration. Tube vulnerable area based on projected tube. Power output, 1 megawatt; tube inside diameter, 3/4 inch; radiator temperature, 1700° R; fin and armor material, beryllium.

Planform Area

Radiator planform area A_p is obtained from the expression

$$A_p = 2Z(L + R_o) = \frac{Q_R}{2\sigma T_b^4 \eta_R^*} \tag{25}$$

Thus, planform area will vary inversely with overall fin-tube thermal effectiveness for a specific choice of power and temperature and will generally increase with increasing L/R_o, since overall fin-tube effectiveness decreases as L/R_o is increased (figs. 12 and 13).

Figure 20(a) illustrates the calculated variations in planform area with L/R_o, N_c, and δ_s/δ_a for maximum Q/W conditions and the same vulnerable area based on a round tube. For the values of conductance parameter obtained for maximum Q/W, the configuration with the minimum planform area corresponds to the configuration for minimum weight.

The closed-sandwich fin-tube planform area results, with tube vulnerable area based on a round tube, are shown in figure 20(b). As the value of δ_s/δ_a decreases, the planform area increases for a specific choice of N_c. Figure 20(c) shows the results of the closed-sandwich fin-tube geometry with tube vulnerable area based on twice the projected tube area. Comparison of these results with those of figure 20(b) shows that little variation in planform area exists with the revised choice of tube vulnerable area.

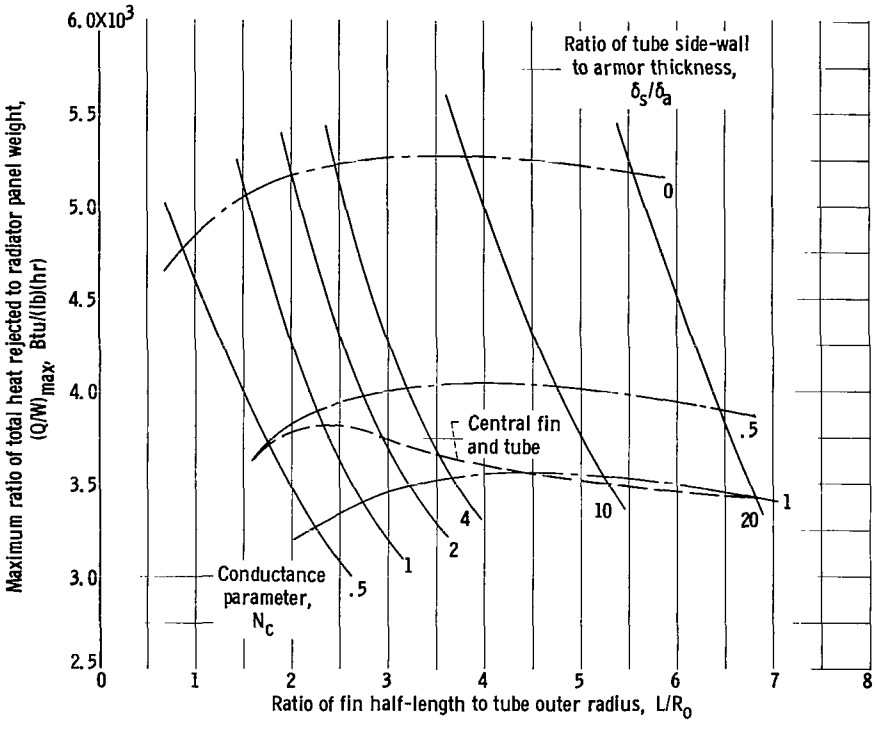

Figure 19. - Comparison of maximum ratio of heat rejected to fin-tube weight for closed-sandwich configuration. Closed sandwich tube vulnerable area based on projected tube.

Fin Thickness

An additional factor of interest with respect to the geometry of the radiator is the magnitude of the fin thickness. Radiator applications might require the fin to have structural or fabricational qualities that could result in nonoptimum weights and dimensions. Fin thickness for the closed-sandwich configurations, or fin half-thickness for the remaining geometries, is obtained from the expression

$$t = \frac{\sigma l^2 T_b^3}{N_c k} \tag{26}$$

Fin thickness as obtained from equation (26) for the maximum Q/W conditions given in figures 15, 17, and 19 is shown plotted in figure 21. Figure 21(a) shows results for total thickness $2t$ for the central-fin and open-sandwich configurations. In the range of minimum weight, the fin thickness $2t$ is of reasonable thickness for all the fin-tube configurations. Lines of constant N_c have not been included in the figure because of the variation of the fin length l of the four configurations.

The fin-thickness results for the closed-sandwich configurations are shown in figure 21(b) for tube vulnerable area based on a round tube and in figure 21(c) for tube vulnerable area twice the tube projected area. The fin thickness obtained is smaller than those of the central-fin and open-sandwich configurations, because the closed sandwich has two fins. Reduction of the tube

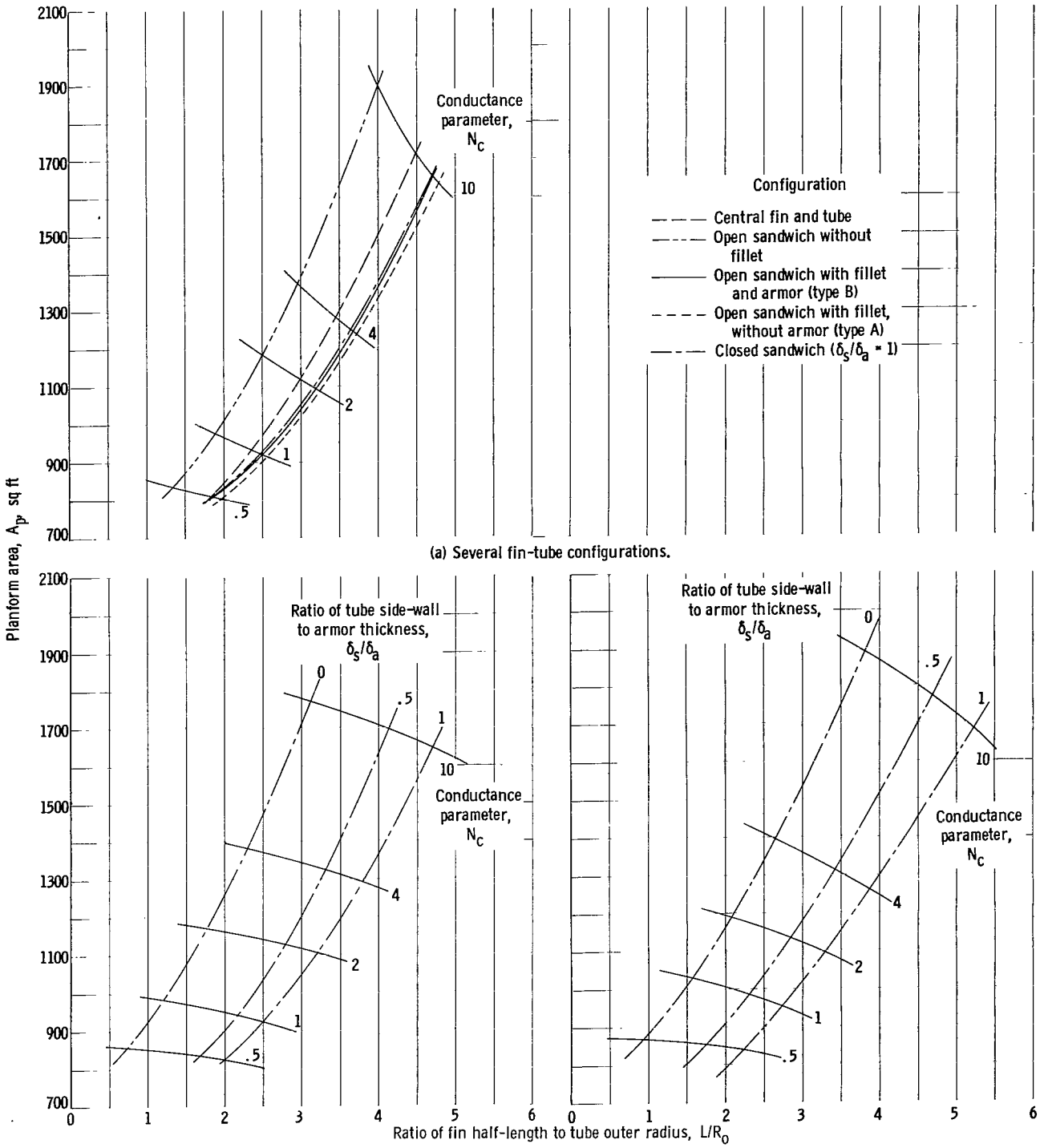

(a) Several fin-tube configurations.

(b) Closed-sandwich fin-tube configurations. Tube vulnerable area based on round tube.

(c) Closed-sandwich fin-tube configurations. Tube vulnerable area based on projected tube.

Figure 20. - Radiator planform area at maximum ratios of heat rejected to radiator panel weight. Power output, 1 megawatt; tube inside diameter, 3/4 inch; radiator temperature, 1700° R; fin and armor material, beryllium.

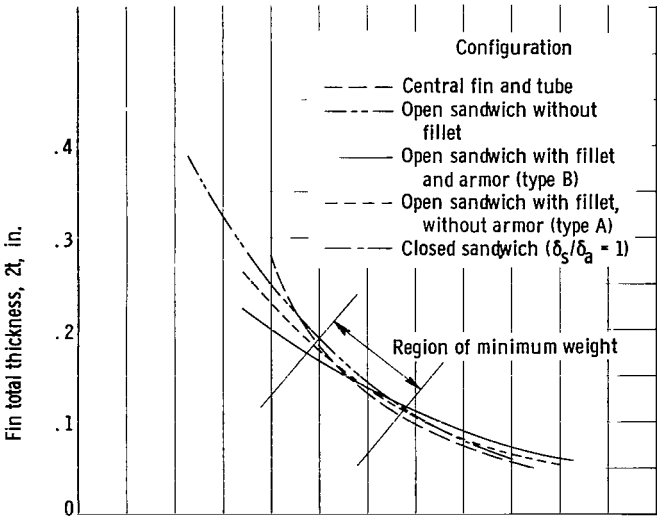

(a) Several fin-tube configurations.

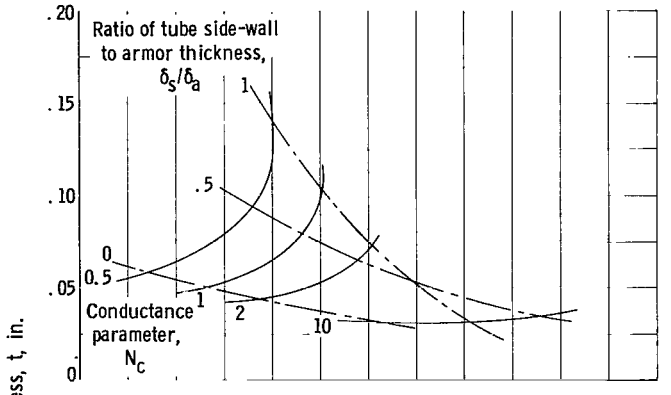

(b) Closed-sandwich configuration. Tube vulnerable area based on round tube.

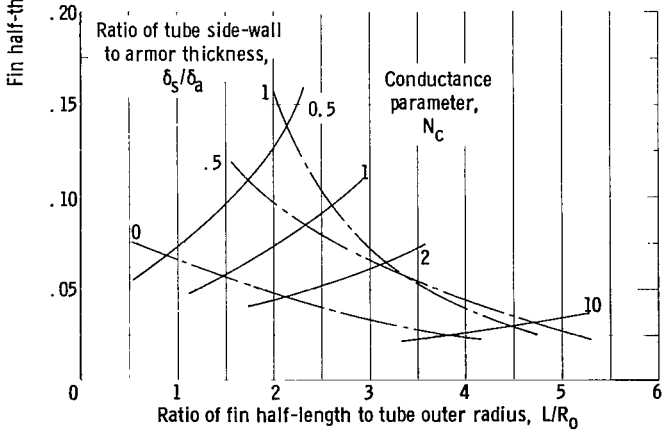

(c) Closed-sandwich configuration. Tube vulnerable area based on projected tube.

Figure 21. - Radiator fin thickness at maximum ratios of heat rejected to radiator panel weight.

side wall substantially reduces the fin thickness at low values of N_c but has little effect at the larger values of N_c, which correspond to minimum weight. The change in model for tube vulnerable area had only a small effect on the fin thickness.

It is conceivable that the fin might act as a structural member of a spacecraft and thus require additional thickness. This would set fin thickness and result in an off-optimum radiator design. An increased fin thickness requires a smaller value of N_c and a smaller L/R_o in order to remain on the Q/W maximum curve given in figures 15, 17, and 19. This would reduce the heat rejected per unit weight and decrease the planform area. This could prove advantageous since, for radiator vehicle integration requiring a reduced planform area, only a small weight penalty would be incurred because the Q/W curves are relatively flat with changing L/R_o.

SUMMARY OF RESULTS

From the analysis of the heat-rejection characteristics of the five fin-tube configurations chosen for this comparison, it has been found that

1. The central fin and tube, the open-sandwich fin and tube with a fillet, and the closed-sandwich configurations with fixed tube side-wall thickness show little variation (less than 7 percent) in overall fin-tube thermal effectiveness for conductance parameters and ratios of minimum fin half-length to tube outer radius of 10 or less.

2. The open-sandwich fin and tube without a fillet and the variable-side-wall closed-sandwich fin-tube configurations exhibit substantially lower fin-tube thermal effectivenesses than those of the geometries mentioned in the earlier case.

Sample heat-rejection and weight calculations for the configurations investigated using a typical 1-megawatt high-temperature Rankine power system showed that

1. The central-fin-and-tube radiator had the highest maximum value of heat rejected per unit weight of the five constant-wall-thickness fin-tube configurations.

2. The open-sandwich fin and tube without a fillet is not a competitive configuration when considered on the basis of heat rejected per unit weight because of its low thermal effectiveness.

3. The closed-sandwich fin-tube configuration with variable side-wall thickness and vulnerable area based on a projected tube offers a weight saving over the conventional central fin if the tube side-wall thickness can be reduced to less than half that required for the exposed surface of the tube.

4. The physical dimensions of a radiator panel (planform area and fin thickness) can be varied over a fairly wide range without seriously decreasing

the radiator heat rejection per unit weight for all configurations.

5. The magnitude of the fin thickness obtained for all the configurations investigated is of a reasonable thickness (greater than 0.030 in. for the closed-sandwich configuration and greater than 0.060 in. for the remaining geometries).

Lewis Research Center
National Aeronautics and Space Administration
Cleveland, Ohio, April 13, 1964

APPENDIX - HEAT-TRANSFER ANALYSIS FOR OPEN SANDWICH WITHOUT FILLET

The analysis is carried out for the open-sandwich fin-tube arrangement of figure 1(b) for the assumptions stated in the text. The law of conservation of energy is applied to a differential element of volume of the fin. Figure 22 shows the element plus the required descriptive angles and dimensions.

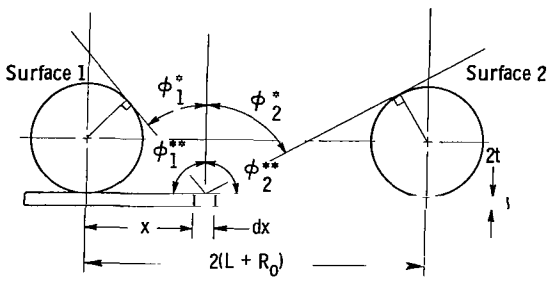

Figure 22. - Schematic drawing of open-sandwich fin and tube without fillet.

Under steady-state conditions, the energy conservation for the fin element consists of a balance between net radiation and conductive transmissions:

$$dQ_{cond,n} + dQ_{rad,n} = 0 \tag{A1}$$

For one-dimensional heat flow in the fin, the net conduction heat transfer per unit length of fin is

$$dQ_{cond,n} = -2kt \frac{d^2T}{dx^2} dx \tag{A2}$$

The net radiation rejected is the difference between the emitted and the incident radiation. The radiant emission for an element is given by the Stefan-Boltzmann law as

$$dQ_{emission} = 2\sigma T^4 \, dx \tag{A3}$$

The incident radiation to the element is contributed from the tubes only, since incident energy from the environment is being neglected for this study. This contribution is

$$dQ_{incident} = \sigma T_b^4 (A_1 F_{1-x} + A_2 F_{2-x}) \tag{A4a}$$

With the use of the reciprocity theorem for angle factors, $A_1 F_{1-x} = dx \, F_{x-1}$ and $A_2 F_{2-x} = dx \, F_{x-2}$. The expression for incident heat becomes

$$dQ_{incident} = \sigma T_b^4 (F_{x-1} + F_{x-2}) dx \tag{A4b}$$

Combining equations (A3) and (A4b) yields the net radiation leaving the element:

$$dQ_{rad,n} = 2\sigma T^4 - \sigma T_b^4 (F_{x-1} + F_{x-2}) dx \tag{A5}$$

Combination of the net radiation (eq. (A5)) expression with the net conduction transfer (eq. (A2)) yields the following form of the energy equation:

$$\frac{d^2T}{dx^2} = \frac{\sigma}{2kt}\left[2T^4 - T_b^4(F_{x-1} + F_{x-2})\right] \tag{A6a}$$

In order to decrease the number of variable parameters, the following dimensionless groups are introduced:

$$\theta = T/T_b$$

$$X = \frac{x}{L + R_o}$$

$$N_c = \frac{l^2\sigma T_b^3}{kt}$$

where $l = L + R_o$. In terms of these new variables, equation (A6) takes the form

$$\frac{d^2\theta}{dX^2} = N_c\left[\theta^4 - \frac{1}{2}(F_{X-1} + F_{X-2})\right] \tag{A6b}$$

The angle factors in equation (A6b) are determined by using figure 22 and a relation that applies to surfaces of infinite length given in reference 6. This general expression for surface 1 is

$$F_{x-1} = \frac{1}{2}(\sin \varphi_1^{**} - \sin \varphi_1^{*}) \tag{A7a}$$

and for surface 2 is

$$F_{x-2} = \frac{1}{2}(\sin \varphi_2^{**} - \sin \varphi_2^{*}) \tag{A8a}$$

Evaluation of these expressions in terms of X and L/R_o yields

$$F_{X-1} = \frac{1}{X^2\left(1 + \frac{L}{R_o}\right)^2 + 1} \tag{A7b}$$

$$F_{X-2} = \frac{1}{(2 - X)^2\left(1 + \frac{L}{R_o}\right)^2 + 1} \tag{A8b}$$

Introduction of expressions (A7b) and (A8b) into equation (A6b) will yield the basic differential equation that describes the temperature profile of the

entire fin. Numerical procedures are used to solve this type of equation with the results shown in figure 7.

The next step is to use the results of the thermal analysis to obtain useful design parametric presentations. A useful result would be the fin effectiveness and the base-surface effectiveness. The fin effectiveness can be calculated by initially obtaining the net heat loss from the fin surface. In steady-state operation, this net heat loss is equal to the heat conducted into the fin at its base. With Q_f defined as the net heat loss from both faces of the fin over the range from $x = 0$ to $x = L + R_o$, the following expression describes the net transfer:

$$Q_f = -2Zkt\left(\frac{dT}{dx}\right)_{x=0} \tag{A9a}$$

Comparing the net heat transfer of the fin with the maximum possible heat transfer from both the fin and the base surface and rewriting the resultant expression in terms of dimensionless variables yield

$$\eta_f^* = \frac{\frac{2Q_f}{Z}}{4\sigma L T_b^4\left(1 + \frac{R_o}{L}\right)} = -\frac{1}{N_c}\left(\frac{d\theta}{dX}\right)_{X=0} \tag{A9b}$$

The base-surface effectiveness is obtained by initially determining the net heat loss from the entire isothermal tube surface:

$$\frac{Q_b}{Z} = \sigma T_b^4 2\pi R_o - \left[2\int_0^{2(L+R_o)} \sigma T^4 F_{x-1}\, dx + \sigma T_b^4 2\pi R_o F_{2-1}\right] \tag{A10a}$$

By introducing symmetry at $X = 1$ on the fin and the previously mentioned dimensionless parameters, equation (A10a) can be rewritten in the form:

$$\frac{\frac{Q_b}{Z}}{4\sigma L T_b^4\left(1 + \frac{R_o}{L}\right)} = \frac{\pi}{2}\frac{1 - F_{2-1}}{1 + \frac{L}{R_o}} - \frac{1}{2}\int_0^1 \theta^4(F_{X-1} + F_{X-2})dX \tag{A10b}$$

where $1 - F_{2-1}$ is obtained from view-factor algebra and is

$$1 - F_{2-1} = \frac{2}{\pi}\left(1 + \frac{L}{R_o}\right)\int_0^1 (F_{X-1} + F_{X-2})dX \qquad (A11)$$

Substitution of equation (A11) into equation (A10b) yields the base-surface thermal effectiveness:

$$\eta_b^* = \frac{\frac{Q_b}{Z}}{4\sigma L T_b^4\left(1 + \frac{R_o}{L}\right)} = \int_0^1 (F_{X-1} + F_{X-2})\left(1 - \frac{1}{2}\theta^4\right)dX \qquad (A12)$$

In this form, the total actual heat loss from the tubes is compared with the maximum possible heat loss from the tube-to-tube span of an isothermal blackbody fin. The integral on the right side of this expression contains the temperature distribution along the fin that was obtained from equation (A6b). The entire fin-tube effectiveness is obtained by adding the results of fin effectiveness (eq. (A9b)) and the base-surface effectiveness (eq. (A12)).

REFERENCES

1. Lieblein, Seymour: Analysis of Temperature Distribution and Radiant Heat Transfer Along a Rectangular Fin of Constant Thickness. NASA TN D-196, 1959.

2. Lin, C. Y.: On Minimum-Weight Rectangular Radiating Fins. IAS J., vol. 27, 1960, pp. 871-872.

3. Bartas, J. G., and Sellers, W. H.: Radiation Fin Effectiveness. J. Heat Trans., ASME Trans., vol. 82, 1960, pp. 73-75.

4. MacKay, D. B., and Leventhal, E. L.: Radiant Heat Transfer from a Flat Plate Uniformly Heated on One Edge. North Amer. Aviation, Inc., Rep. MD 58-187, Aug. 1958.

5. Wilkins, J. E.: Minimum Mass Thin Fins for Space Radiators. Proceedings of the 1960 Heat Transfer and Fluid Mechanics Institute, pp. 229-243.

6. Sparrow, E. M., and Eckert, E. R. G.: Radiant Interaction Between Fin and Base Surfaces. J. Heat Trans., ASME Trans., vol. 84, 1962, pp. 12-18.

7. Haller, Henry C., Wesling, Gordon C., and Lieblein, Seymour: Heat-Rejection and Weight Characteristics of Fin-Tube Space Radiators with Tapered Fins. NASA TN D-2168, 1964.

8. Walker, C. L., Smith, C. R., and Gritton, D. G.: Weight Optimization of Heat Rejection Systems for Space Applications. Proceedings of the 1960 Heat Transfer and Fluid Mechanics Institute, pp. 244-259.

9. Callinan, J. P., and Berggren, W. P.: Some Radiator Design Criteria for Space Vehicles. J. Heat Trans., ASME Trans., vol. 81, 1959, pp. 237-244.

10. Diamond, P. M., and Hopson, G. D.: Heat Rejection in Space. Pt. 5 of Short Course in Space Power Plants, Univ. Calif., July 1961.

11. Haller, H. C., and Stockman, N. O.: A Note on Fin-Tube View Factors. J. Heat Trans., ASME Trans., vol. 85, 1963, p. 380.

12. Sparrow, E. M., and Minkowycz, W. J.: Heat-Transfer Characteristics of Several Radiator Finned-Tube Configurations. NASA TN D-1435, 1962.

13. Loeffler, I. J., Lieblein, S., and Clough, N.: Meteoroid Protection for Space Radiators. Progress in Astronautics and Aeronautics, Power Systems for Space Flight, vol. 11, Academic Press, 1962, pp. 551-579.

2/7/87
S

"The aeronautical and space activities of the United States shall be conducted so as to contribute . . . to the expansion of human knowledge of phenomena in the atmosphere and space. The Administration shall provide for the widest practicable and appropriate dissemination of information concerning its activities and the results thereof."

—NATIONAL AERONAUTICS AND SPACE ACT OF 1958

NASA SCIENTIFIC AND TECHNICAL PUBLICATIONS

TECHNICAL REPORTS: Scientific and technical information considered important, complete, and a lasting contribution to existing knowledge.

TECHNICAL NOTES: Information less broad in scope but nevertheless of importance as a contribution to existing knowledge.

TECHNICAL MEMORANDUMS: Information receiving limited distribution because of preliminary data, security classification, or other reasons.

CONTRACTOR REPORTS: Technical information generated in connection with a NASA contract or grant and released under NASA auspices.

TECHNICAL TRANSLATIONS: Information published in a foreign language considered to merit NASA distribution in English.

TECHNICAL REPRINTS: Information derived from NASA activities and initially published in the form of journal articles.

SPECIAL PUBLICATIONS: Information derived from or of value to NASA activities but not necessarily reporting the results of individual NASA-programmed scientific efforts. Publications include conference proceedings, monographs, data compilations, handbooks, sourcebooks, and special bibliographies.

Details on the availability of these publications may be obtained from:

SCIENTIFIC AND TECHNICAL INFORMATION DIVISION

NATIONAL AERONAUTICS AND SPACE ADMINISTRATION

Washington, D.C. 20546